Available online at www.sciencedirect.com
ScienceDirect
Applied Catalysis B: Environmental 83 (2008) 177–185
APPLIED CATALYSIS B: ENVIRONMENTAL
www.elsevier.com/locate/apcatb

Tungsten and nitrogen co-doped TiO_2 nano-powders with strong visible light response

Yanfang Shen [a,b], Tianying Xiong [a,*], Tiefan Li [a], Ke Yang [a]

[a] *Institute of Metal Research, Chinese Academy of Sciences, Shenyang 110016, China*
[b] *Graduate School of Chinese Academy of Sciences, Beijing 100086, China*

Received 10 May 2007; received in revised form 27 January 2008; accepted 29 January 2008
Available online 15 February 2008

Abstract

A two-step method, combining with sol–gel and mechanical alloying (MA) method, was used to fabricate the tungsten and nitrogen co-doped TiO_2 nano-powders ((W, N) co-doped TiO_2 NPs). The (W, N) co-doped TiO_2 NPs showed strong absorbance in visible range, as long as 650 nm. Enhanced photocatalytic activities under visible light irradiation were also observed from the results of photodegradation experiments and chemical oxygen demand (COD) analysis. Physical, chemical, and optical properties of the samples were investigated. Possible reasons for the enhanced photocatalytic activities were analyzed based on the experimental results. Oxygen vacancies detected by electron spin response (ESR) spectra, acting as trapping agencies for electrons (e^-) to produce active oxygen species ($^{\bullet}O^{2-}$), were proved to be the main cause for the improved photocatalytic performances.

Keywords: TiO_2; Co-doped; Two-step method; COD

1. Introduction

Titanium dioxide (TiO_2) has been studied extensively as a kind of efficient photocatalyst for its excellent properties, such as non-toxicity, high thermal-stability and low cost [1–3]. However, TiO_2 photocatalysts can be excited only by expensive ultraviolet (UV) light, because of the large band gap of 3.0–3.2 eV [4]. In order to conserve energy and make full use of the solar energy, visible light is considered as an ideal exciting light source for TiO_2 photocatalysts. Thus, currently a hot research field on TiO_2 photocatalysts is to make the threshold of the absorption spectra red-shifted and enlarged, so that a high ratio of the usage of visible light can be conducted.

Visible light sensitive TiO_2 photocatalysts have been investigated by many researchers and several approaches have been proved to be effective to some extent. Modification of TiO_2 photocatalysts with metal ions was extensively studied [5–8]. A systematic study of metal ion doping in TiO_2 colloids was carried out by Choi et al. [9]. It was found out that the photoreactivity of TiO_2 colloids for both oxidation and reduction can be enhanced by doping with Fe^{3+}, Mo^{5+}, Ru^{3+}, Os^{3+}, Re^{5+}, V^{4+} and Rh^{3+} at 0.1–0.5 at%, while reduced photoreactivities were observed in Co^{3+} and Al^{3+} doped TiO_2 colloids.

Besides metal ions, some non-metal ions, such as C [10,11], N [12–14], S [15,16], F [17] and P [18] were also used as dopants in the modification of TiO_2 photocatalysts. Asahi et al. [12] prepared films and powders of $TiO_{2-x}N_x$ by sputtering the TiO_2 target in an N_2 (40%)/Ar gas mixture and annealing anatase TiO_2 powders in the NH_3 (67%)/Ar atmosphere, respectively. It was reported that the $TiO_{2-x}N_x$ samples were superior to its TiO_2 counterpart under visible light irradiation although both the samples showed similar UV activities, when methylene blue (MB) and gaseous acetaldehyde were chosen as photodegradation targets. First-principle calculations were also carried out to approximate the possibilities of non-metal doping.

Though there are a lot of literatures about the metal ions doped TiO_2 and the non-metal ions doped TiO_2, reports on the metal ions and non-metal ions co-doped TiO_2 photocatalysts are seldom. Sakatani et al. [19] prepared the metal ions and nitrogen co-doped TiO_2 powders by a polymerized complex

* Corresponding author.
E-mail address: tyxiong@imr.ac.cn (T. Xiong).

0926-3373/$ – see front matter © 2008 Published by Elsevier B.V.
doi:10.1016/j.apcatb.2008.01.037

method. Several metal ions were studied, including K^+, Ca^{2+}, Sr^{2+}, Ba^{2+}, Nb^{5+}, Fe^{3+}, Zn^{2+}, and Al^{3+}. Of them all, the photocatalysts of Sr^{2+} and nitrogen co-doped TiO_2 exhibited the highest activities in the decomposition of acetaldehyde under visible light illumination. It was suggested that the formation of paramagnetic N species at interstitial positions in the TiO_2 lattice was responsible for the visible light response of the catalyst.

In the present report, tungsten and nitrogen co-doped TiO_2 NPs were prepared. And the behavior of the (W, N) co-doped TiO_2 NPs in the photodegradation of methylene blue (MB) and sulfosalicylic acid (SSA) using visible light excitation was investigated. The study is intended to give a picture of physical and chemical properties of this kind of photocatalyst and the influence of the amounts of W and N on the photocatalytic reactions, which is a reference when synthesis of other metal and non-metal co-doped TiO_2 by this method.

2. Experimental

2.1. Preparation of (W, N) co-doped TiO_2

The (W, N) co-doped TiO_2 NPs were prepared by a two-step method. In the first step, tungsten doped TiO_2 nano-powders (W-doped TiO_2 NPs) were prepared by the sol–gel technique as follows. Tetrabutyl titanate (TTOB, 34 ml) and ethanol (EtOH, 88 ml) were mixed together with strong stirring for 30 min, and then 1.4 ml of nitrate (HNO_3, 70 wt%) was added. Consequently different amount of Na_2WO_4 aqueous solution was added drop-wise. The amount of W added varied from 0.5 to 10 wt%. After 2-day gelation at room temperature, the obtained gel was dried at 60 °C. The dried gel was then calcined at 600 °C to obtain the W-doped TiO_2 NPs.

In the second step, urea and the obtained W-doped TiO_2 powders were ball-milled together in a 50-ml agate vessel. The procedures were described firstly by Yin and co-workers [20]. Considering that the process parameters play an important role in the nature and kinetics of the product phase obtained by mechanical alloying (MA), most of the parameters, such as the milling temperatures, milling time, grinding ball diameter, ball-to-powder weight ratio and relative proportion of the reactants, were kept constant in the present work. Besides, no other process control agencies (PCA) were used. In the work, the weight ratio of W-doped TiO_2 and urea was 10:1, and the milling time was 5 h. After MA, the milled powders were calcined in the flowing N_2 atmosphere at 400 °C for 1 h to remove the residual urea.

2.2. Characterization

The purity and crystallinity of the prepared samples were examined by powder X-ray diffraction (XRD) using an X-ray diffractometer with Cu Kα radiation (λ = 1.5418 Å). The average crystallite size was calculated using the Scherre's equation [21].

Raman spectrum analysis was conducted on a Labram HR800 Laser Raman Spectroscopy made by Jobin Yvon, France, using the 632.8-nm He–Ne ion laser as an excitation source. The laser power on the sample was 10 mW.

Morphologies of the samples were investigated on a JEOL 2010 Field Emission Electron Microscope. The samples were dispersed in ethanol solution using ultrasonic, and then dropped on carbon-coated copper collars.

N_2 adsorption–desorption analysis was conducted on an ASAP 2010 Surface Area and Porosity Analyser made by Micrometritics Instrument Corporation, USA, to get the Brunauer–Emmett–Teller (BET) surface area, mesopore volume and size distribution by Barrett–Joyner–Halenda (BJH) method.

X-ray photoelectron spectra (XPS) of the samples were measured using a PHI5300 photoelectron spectrometer system with an Al Kα source (1486.6 eV). The shift of binding energy due to relative surface charging was corrected using the C 1s level at 284.6 eV as an internal standard of the surface adventitious carbon.

FTIR spectra on pellets of the samples mixed with KBr were recorded on a MATNA-IR 560 (made by Nicolet, USA) spectrometer.

The electron spin response (ESR) spectra were recorded at room temperature using a JEOL JES-FE3AX ESR spectrometer.

UV–vis spectrum analysis was measured using a Jasco V-550 spectrophotometer.

2.3. Photocatalytic reactions

The photocatalytic activities of the received samples were evaluated by measuring both the photodiscoloration of MB and the photodegradation of SSA under visible light. A 13-W fluorescent lamp was used as the visible light source. About 95% of the radiant energy in the electromagnetic spectrum of the fluorescent lamp is in visible light region, and the other 5% in the ultraviolet light region. A light filter was employed to exclude the disturbance of ultraviolet light. The distance between the strip lamp and fluid level was kept as 10 cm. The initial concentrations of the solutions of MB and SSA were 20 and 40 mg/l, respectively. And the amounts of the samples added into the MB solution and SSA solution were 0.5 and 1 g/l, respectively. Before the light was on, the target solution was stirred for 30 min in the dark until adsorption-desorption balance was reached on the sample. Degussa P25 was used as a reference.

To evaluate the mineralization degree of the (W, N) co-doped TiO_2 samples in MB discoloration, COD analysis was conducted just after the photodiscoloration experiments. After the experiments, a proper amount of the remained solution was adopted and filtered by macromolecular films. Then, the clarified MB solution was analyzed according to the potassium dichromate method [22], and denoted as COD_{Cr}.

2.4. Labels of the prepared samples

The (W, N) co-doped TiO_2 samples were named as *n*-NWT series, and the W-doped TiO_2 were named as *n*-WT series,

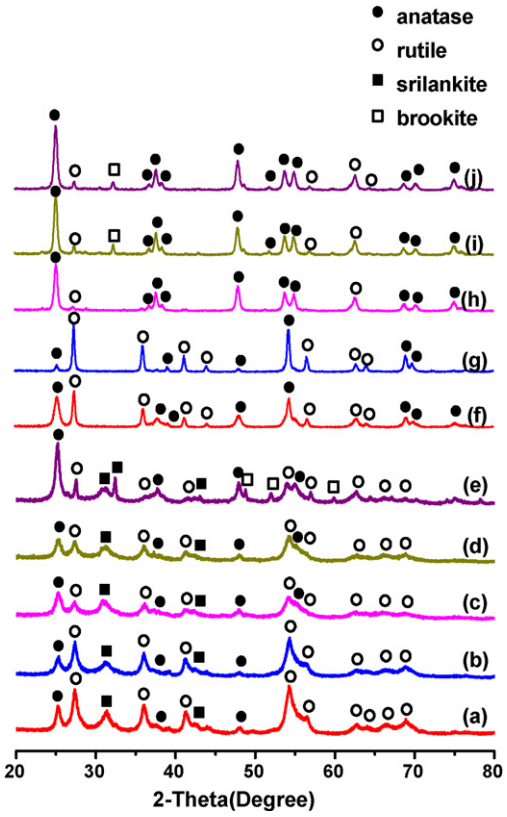

Fig. 1. XRD patterns of the prepared samples: (a) 0.5 wt%NWT; (b) 1 wt%NWT; (c) 3 wt%NWT; (d) 5 wt%NWT; (e) 10 wt%NWT; (f) 0.5 wt%WT; (g) 1 wt%WT; (h) 3 wt%WT; (i) 5 wt%WT; (j) 10 wt%WT.

where n represents the weight fraction of W added in the producing procedures.

3. Results

The XRD patterns of the prepared samples are presented in Fig. 1. Usually, anatase, rutile and brookite are the three common phases of TiO_2. Brookite is a transitional phase from anatase to rutile in the healing processes. Besides the above three phases, srilankite is also detected as a phase of TiO_2, which is a high-pressure modification belonging to α-PbO_2 type. It can be seen from Fig. 1 that the (W, N) co-doped TiO_2 NPs are mixed crystals of anatase, rutile, srilankite and brookite. While the phases of anatase, rutile and brookite are presented in the W-doped TiO_2 NPs, no srilankite is detected. Therefore it can be suggested that the srilankite in the (W, N) co-doped TiO_2 NPs was formed in the ball-milling processes, during which the powders were repeatedly welded, fractured and re-welded. The BET surface areas and the secondary particle sizes calculated from BET data of the (W, N) co-doped TiO_2 NPs were listed in Table 1. It is easy to find out that the higher the concentration of W in the (W, N) co-doped TiO_2, the larger the BET surface area, and the smaller the corresponding crystal size. This indicates that doping with tungsten can hinder the phase transition from anatase to rutile, and confine the crystal growth meanwhile, which may be benefit for the photoactivity of (W, N) co-doped TiO_2.

Table 1
BET surface areas and the secondary particle sizes of (W, N) co-doped TiO_2 NPs

	Samples				
	0.5 wt%NWT	1 wt%NWT	3 wt%NWT	5 wt%NWT	10 wt%NWT
BET (m^2/g)	78.29	79.74	84.56	88.86	94.94
d_{BET} (nm)	20.2	19.8	18.7	17.8	16.6

Raman spectra of the (W, N) co-doped TiO_2 powders are shown in Fig. 2. Optical Raman spectroscopy is a powerful tool in the study of TiO_2 for its high sensitivity to the microstructure. It can be seen from Fig. 2 that the typical Raman peaks of anatase, rutile and brookite are detected in each sample according to the previous work, which reports that the characteristic Raman peaks of anatase locate at 144, 320, 399, 515 and 639 cm^{-1}, rutile gives scatterings at 143, 235, 447 and 612 cm^{-1}, while brookite shows the peaks at 128, 153, 172, 247, 322, 366, 427 and 636 cm^{-1} [23–25]. Taken the sample of 0.5 wt%NWT for example, it reveals seven Raman active bands for the sample of 0.5 wt%NWT, of which 144, 316, 516 and 639 cm^{-1} are in agreement with data on anatase [26], 172 and 427 cm^{-1} belong to brookite, and 441 cm^{-1} to rutile [26], respectively. The characteristic Raman peaks for WO_3 were observed at 807, 715, 324, 293, and 270 cm^{-1} [27]. Interestingly, the Raman spectra in the present work did not show any trace of WO_3, implying that the amount of WO_3 was too low to be checked out. This is also in agreement with the XRD results.

The OH bonding characteristics of water molecules associated with the surface polar hydroxyl groups of 0.5 wt%NWT and 1 wt%NWT are given as models in Fig. 3, and both possess similar vibrations in the IR region. The intensive and broad bands at 550–635 cm^{-1}, peaking at 636.4 cm^{-1}, were ascribed to the stretching vibrations of Ti–O bond [28,29]. The intensive bands of OH^- group stretching at 3200–3550 cm^{-1} (O–H) and the deformation vibrations at 1600–1630 cm^{-1} (H–O–H) were observed on the spectra, which was an evidence of a large amount of water molecules absorbed on the surface of TiO_2 [30]. The absorption locating at

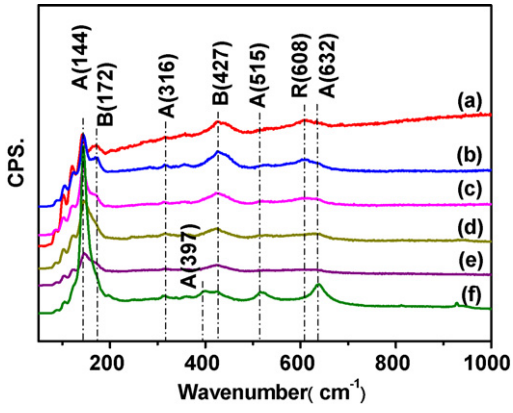

Fig. 2. Raman spectra of the prepared samples: (a) 0.5 wt%NWT; (b) 1 wt%NWT; (c) 3 wt%NWT; (d) 5 wt%NWT; (e) 10 wt%NWT; (f) P25.

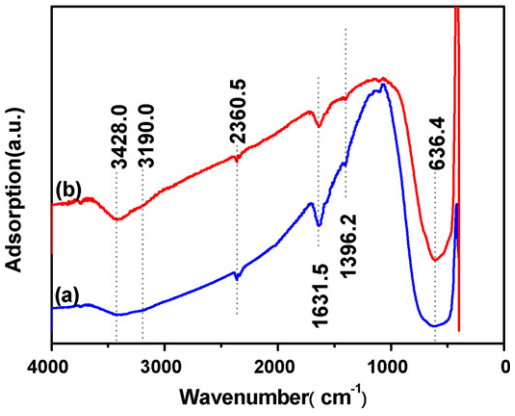

Fig. 3. FTIR spectra of the prepared samples: (a) 0.5 wt%NWT; (b) 1 wt%NWT.

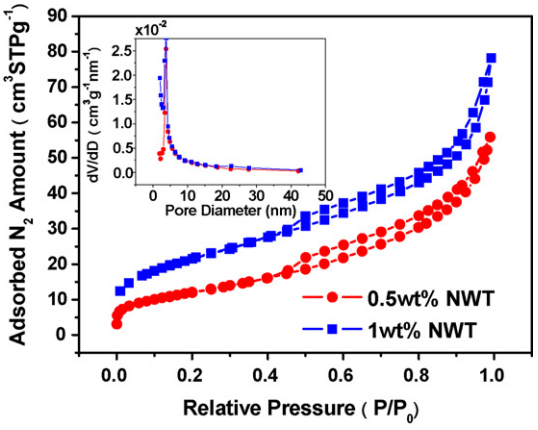

Fig. 5. N_2 adsorption–desorption isotherms and the pore size distributions (inset): (a) 0.5 wt%NWT; (b) 1 wt%NWT.

3428 cm^{-1} characterizes the weak surface active sites with which the physically absorbed water molecules are bound by weak hydrogen bonds, while the weak absorption locating at 3190 cm^{-1} corresponds to the chemically absorbed water complexes that are strongly bound to the surface of TiO_2. As to the absorption at 1631.5 cm^{-1}, it is associated with the deformation vibrations of physically absorbed water molecules. The presence of large amount hydroxyl groups was considered beneficial for the photocatalytic process. On the one hand, the hydroxyl groups may accept h^+ when irradiated with light, producing $^{\bullet}OH^-$ which possesses high oxidizability. On the other hand, the surface hydroxyl groups can also act as absorption centers for O_2, CO_2 and CO molecules [30]. Besides, the IR band at 2360.5 cm^{-1} is the characteristic of the stretching vibrations of N–H bond, which is the result of nitrogen doping [31], while the presence of the IR band of 1396.2 cm^{-1} is an evidence of the absorbed molecular oxygen [30].

TEM images of the (W, N) co-doped TiO_2 are shown in Fig. 4. It is seen that the secondary particles of the samples of 0.5 wt%NWT and 1 wt%NWT are approximately spherical in shape. And the average particle sizes of the prepared samples are about 20 nm.

The N_2 adsorption–desorption isotherms of 0.5 wt%NWT and 1 wt%NWT are shown in Fig. 5. Inside is the pore size distribution of the two samples. Both the samples show similar N_2 adsorption and desorption isotherms. According to IUPAC [32], it is seen that the adsorption isotherm belongs to Type II, while the desorption isotherm belongs to Type IV. Therefore it can be consumed that the particle size of the prepared samples was mainly distributed in the mesoporous range [33]. A clear hysteresis loop at high relative pressure is observed, which is related to the capillary condensation association with large pore channels. The pore size distribution of the prepared samples was approximately 4 nm according to the BJH solutions of the desorption curves.

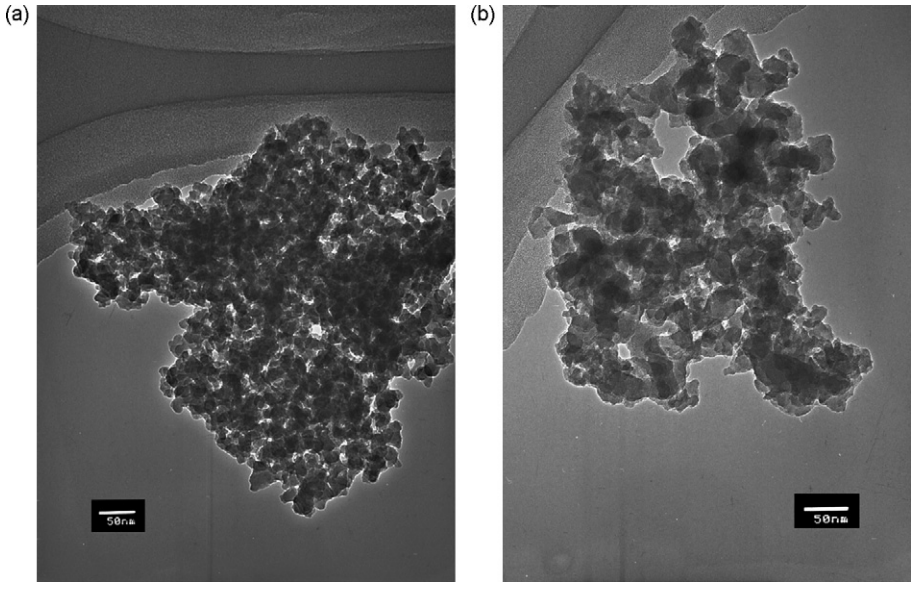

Fig. 4. TEM images of the prepared sample: (a) 0.5 wt%NWT; (b) 1 wt%NWT.

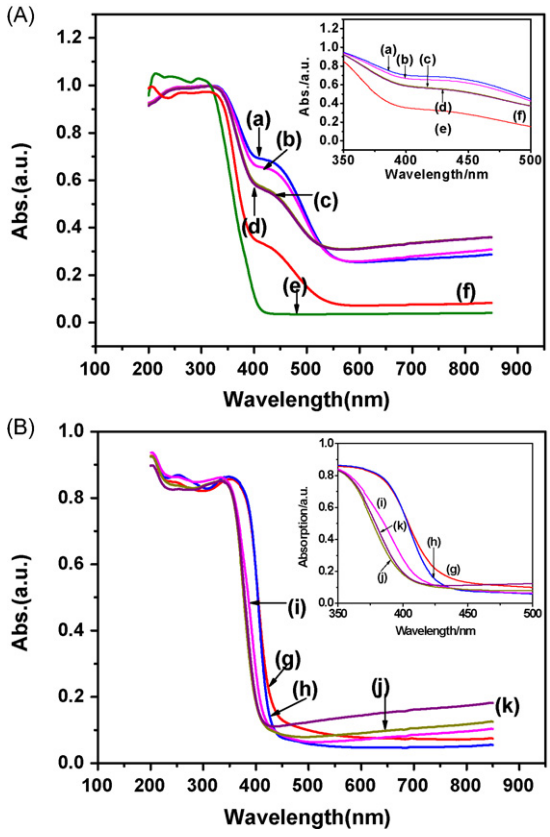

Fig. 6. (A) Diffuse-reflectance spectra of the prepared (W, N) co-doped TiO_2 NPs and commercial Degussa P25: (a) 0.5 wt%NWT; (b) 1 wt%NWT; (c) 3 wt%NWT; (d) 5 wt%NWT; (e) 10 wt%NWT; (f) P25. (B) Diffuse-reflectance spectra of the W-doped TiO_2 NPs: (g) 0.5 wt%WT; (h) 1 wt%WT; (i) 3 wt%WT; (j) 5 wt%WT; (k) 10 wt%WT. The inset shows the details of the DRS spectra in the range of 350–500 nm.

It is seen from Fig. 6(A) that there exist two adsorption edges in the DRS curves of the prepared (W, N) co-doped TiO_2 NPs. The first edge (400–500 nm) is thought to be related to the natural width of energy level (Table 2). The second one is around 600 nm, which is in the visible range, indicating that the new energy levels are successfully formed in the forbidden band of TiO_2. According to Asahi's method [12], the absorption edge of (W, N) co-doped TiO_2 NPs can be located at 650 nm, which indicates that the light with wavelength shorter than 650 nm can be absorbed by the samples. In the samples of (W, N) co-doped TiO_2 NPs, 3 wt%NWT possesses the best absorption ability in the visible light range. As to those W-doped TiO_2 NPs, there is only one adsorption shoulder in the spectrum, locating in the UV region. Although the W-doped TiO_2 NPs can adsorb some visible light as well, the adsorpted amount is not as large as the (W, N) co-doped TiO_2 NPs.

In order to analyze the chemical states of the prepared samples, XPS spectra were detected and shown in Fig. 7. The global range XPS spectra of the co-doped NPs were presented in Fig. 7(A). It is clear that both the W and N were detected even after the etching with Ar^+ for 30 s, which suggests that both the elements were doped into the lattice of TiO_2. The W 4f peaks of the prepared samples locate at about 37 eV as shown in Fig. 7(B). The N 1s binding energy peaks are broad, extending from 397 to 402 eV, as shown in Fig. 7(C). The center of the N 1s peak locates at about 399.7 eV, which is attributed to the formation of O–Ti–N bond [34]. Compared with the previous literatures, the value is higher than Asahi's [12], who reported that the intensity of N 1s peak located at 396 eV in N-doped TiO_2 NPs. Besides Asahi's work, some other researches [35–37] also reported the enhanced photocatalytic properties under visible light due to the nitrogen doping, with N 1s peaks centering at 396 eV in the XPS spectra. However, the N 1s peak was not always locating at 396 eV, and there were some reports that pointed out that the N 1s peak positioned at about 399.6 eV was responsible for the visible light response in their work. Sakthivel et al. [38] prepared N-doped TiO_2 from titanium tetraisopropoxide or titanium tetrachloride and thiourea, and they found out that the most intense N 1s peak (the sample was sputtering with Ar^+ for 30 s) located at 400.1 eV, and there also existed two less intense peaks at 405 and 411.8 eV. Gole et al. [39] prepared the $TiO_{2-x}N_x$ photocatalysts by employing the direct nitridation of anatase TiO_2 nanostructures with alkylammonium salts, and then treated the N-doped TiO_2 with palladium salts to introduce Pd. They reported that the N 1s peak centered at 400.7 eV for both the $PdCl_2$ treated and untreated $TiO_{2-x}N_x$, and a distinct peak located at 406.5 eV for $Pd(NO_3)_2$-treated aminated samples. Taking into account of all the above results, it can be presumed that the N 1s binding energy may vary from case to case when the $TiO_{2-x}N_x$ is prepared using different methods. This is in agreement with Chen and Burda [34], who also suggest that the shifting of N 1s peak can be understood by the fact that the N 1s binding energy

Table 2
Absorption edges and band gap energies of the samples

Preparation conditions	First absorption edge (nm)	First band gap energy (eV)	Second absorption edge (nm)	Second band gap energy (eV)
As-received P25	420	2.95	None	None
0.5 wt%NWT	530	2.34	625	1.98
3 wt%NWT	500	2.48	650	1.91
5 wt%NWT	495	2.50	655	1.89
10 wt%NWT	425	2.92	600	2.07
0.5 wt%WT	450	2.76	None	None
1 wt%WT	440	2.82	None	None
3 wt%WT	420	2.95	None	None
5 wt%WT	410	3.02	None	None
10 wt%WT	415	2.99	None	None

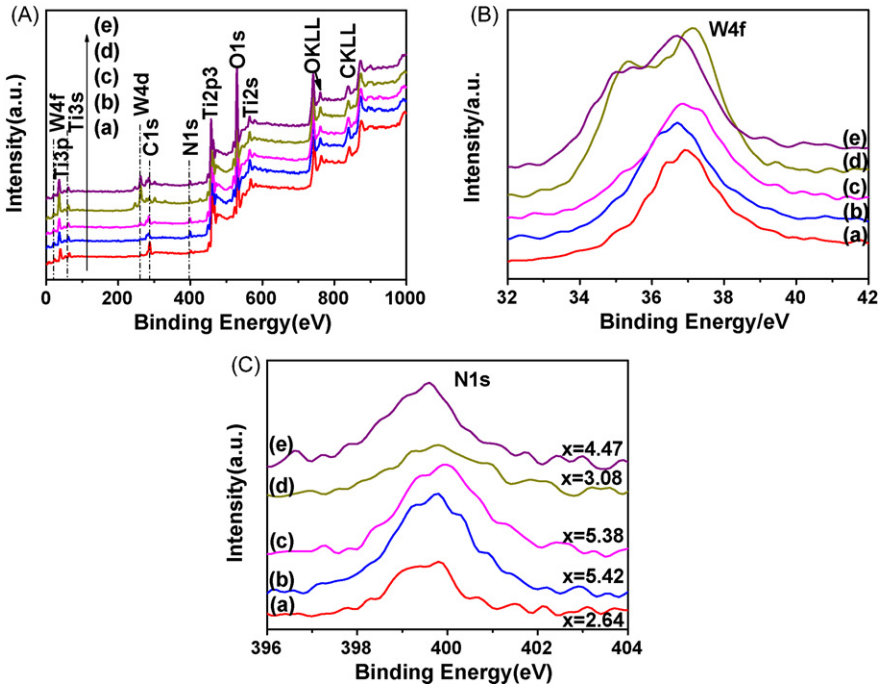

Fig. 7. (A) Comparisons of the global range X-ray photoelectron spectra of the (W, N) co-doped TiO_2 samples; (B) N 1s peak of the samples around the 400 eV region; (C) W 4f peak of the samples around the 37 eV region. Sample index in the spectra: (a) 0.5 wt%NWT; (b) 1 wt%NWT; (c) 3 wt%NWT; (d) 5 wt%NWT; (e) 10 wt%NWT. The spectra were measured after the surface of the powders was etched with Ar^+ for 30 s to remove the absorbed contaminations.

is higher when the formal charge is more positive (e.g. 408 eV in $NaNO_3$) than zero (e.g. 400 and 402 eV in γ-N_2) or a negative formal charge (e.g. 398.8 eV in NH_3 and 396 V in β-N of TiN).

Kinetic curves of photodiscoloration of MB under visible light irradiation in the presence of the (W, N) co-doped samples and P25 are shown in Fig. 8. The (W, N) co-doped TiO_2 NPs showed much enhanced photocatalytic activities than that of Degussa P25. Of them all, 3 wt%NWT showed the highest photocatalytic activity than others. Fig. 9 gives the absorption curves of MB detected at 660 nm in the presence of 3 wt%NWT under visible light irradiation. The gradual decrease of the absorption of MB over time is attributed to the changes of the molecular structure of the dye, which proves the direct photodegradation in turn. The simplified Langmuir–Hinshelwood forms, $\ln(C_0/C) = kKt = K't$, at different initial concentrations, the initial concentrations, C_0, and the MB degradation rates, $(C_0 - C)/C_0$, are shown in Table 3. It can be seen from Table 3 that the MB solution showed different concentrations after they were laid aside in the dark to reach the adsorption–desorption balance, although the concentrations were all kept at 20 mg/l before the samples were added. Besides, the MB degradation rates, $(C_0 - C)/C_0$, increased with the decreasing of the initial concentration, C_0. This indicates that the samples with strong adsorptive capacity show higher photocatalytic activities.

Presented in Fig. 10 are the COD_{Cr} removing rates of the (W, N) co-doped TiO_2 NPs and P25. Similar with the experimental

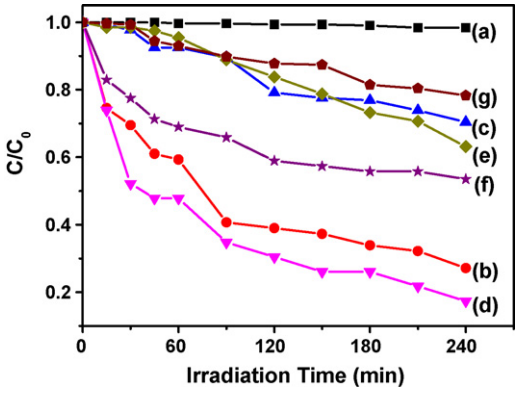

Fig. 8. Kinetic curves of photodiscoloration of MB in the presence of visible light, as monitored by changes in the absorbance at 660 nm: (a) blank; (b) 0.5 wt%NWT; (c) 1 wt%NWT; (d) 3 wt%NWT; (e) 5 wt%NWT; (f) 10 wt%NWT; (g) P25.

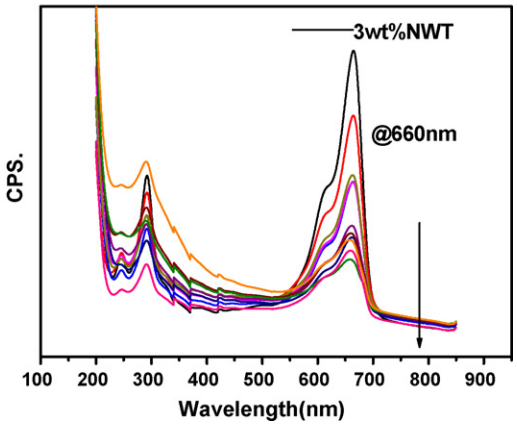

Fig. 9. The adsorption curves of MB during the photodiscoloration process using 3 wt%NWT in water at neutral pH.

Table 3
Simplified Langmuir–Hinshelwood form, $\ln(C_0/C) = kKt = K't$, at different initial concentrations

Samples	C_0 ($\times 10^{-5}$ M)	Simplified Langmuir–Hinshelwood form	$(C_0 - C)/C_0$
Blank	3.14	$\ln(C_0/C) = -0.00189 + 7.15903 \times 10^{-5}t$	0.01592
P25	2.86	$\ln(C_0/C) = -0.0025 + 0.00106t$	0.21378
0.5 wt%NWT	0.59	$\ln(C_0/C) = 0.23111 + 0.00481t$	0.72881
1 wt%NWT	1.34	$\ln(C_0/C) = -0.15643 + 0.00413t$	0.29597
3 wt%NWT	0.23	$\ln(C_0/C) = 0.323 + 0.00621t$	0.82609
5 wt%NWT	1.98	$\ln(C_0/C) = -0.03951 + 0.00192t$	0.36869
10 wt%NWT	1.29	$\ln(C_0/C) = 0.17558 + 0.0022t$	0.46512

result on the color-bleaching, 3 wt%NWT showed best COD_{Cr} removing abilities, and the CODCr removing rate of which was as high as 97.39%. Besides, other (W, N) co-doped TiO_2 also showed higher COD_{Cr} removing rates than that of P25, only 48.63%. However, the varying tendencies of the color-bleaching rates do not always keep in agreement with the COD_{Cr} removing rates in the experiments. For example, the sample of 0.5 wt%NWT appeared to be the second-best photocatalyst in the six samples when only the color-bleaching rate was considered, while, it ranked as the forth when COD_{Cr} removing rate was checked. Thus, it is suggested that the COD values should also be detected as compensation in the photodegradation experiments of dyes.

Kinetic curves of photodegradation of SSA under visible light irradiation are shown in Fig. 11. Much enhanced photocatalytic activities are observed on the samples. The photodegradation rates of 3 wt%NWT and 10 wt%NWT reach 49.0% and 67.1%, respectively, which are about 5 and 7 times of that of Degussa P25. The absorption curves of SSA detected at 297.5 nm in the photodegradation experiment using the sample of 10 wt%NWT are presented in Fig. 12. The intensity of the absorption curve reduces as the decreasing of the concentration of SSA solution, which is supposed to be the result of the changes of the benzene ring in the molecular structure of SSA.

The initial concentration of SSA solution, photodegradation rates of the samples and the amount of SSA absorbed on the samples are listed in Table 4. It is seen that the samples with better absorbance abilities exhibit enhanced photodegradation rates, suggesting that the absorbance of SSA on the surfaces of the samples is beneficial for the photodegradation actions. The probable reason is that SSA absorbed on the samples can be attacked directly by hydroxyl radicals ($^{\bullet}OH^{-}$) and super oxygen ($^{\bullet}O^{2-}$), compared with those disturbed in solution.

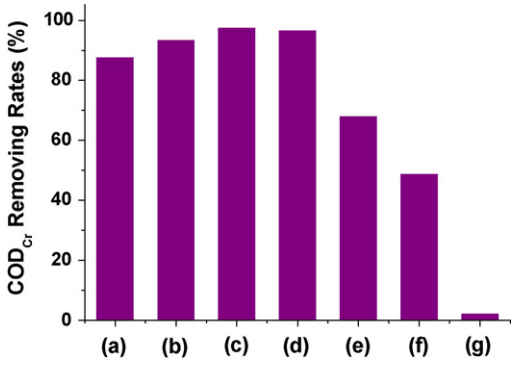

Fig. 10. Comparison of the COD_{Cr} removing rate of the samples after irradiation under visible light for 4 h: (a) 0.5 wt%NWT; (b) 1 wt%NWT; (c) 3 wt%NWT; (d) 5 wt%NWT; (e) 10 wt%NWT; (f) P25; (g) blank.

4. Discussion

4.1. Impact of MA in phase transformation and nitrogen doping

MA is a solid-state powders processing technique involving repeated welding, fracturing and re-welding of powder particles in a high-energy ball miller. A characteristic feature of all solid-state reactions is the formation of product phase(s) at the interfaces of the reactants [40]. Normally, anatase transforms to rutile at about 600 °C, and improvement of the calcinating temperatures often induces large crystal sizes, agglomeration of particles and low BET surface areas, which are disadvantageous for photocatalytic reactions. During the MA process, the repeated welding and fracturing of powder particles usually increase the area of contact between the reactant powder particles due to the reduction of particle size and allow fresh surfaces to come into contact repeatedly. As a consequence, phase transformations that normally require higher temperatures can occur at lower temperatures during MA process without any extra heat. Besides, a large amount of defects, such as vacancies and dislocations could be induced into TiO_2, which can accelerate the atom diffusion process greatly.

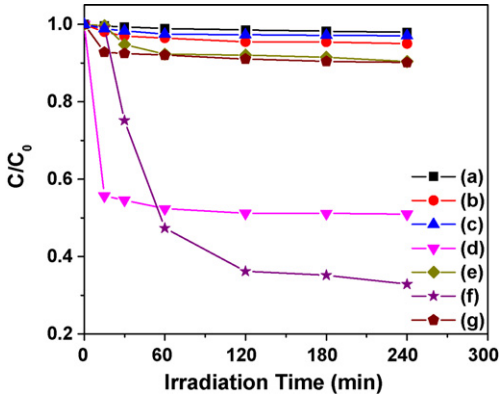

Fig. 11. Kinetic curves of photodegradation of SSA under visible light, as monitored by changes in the absorbance at 297.5 nm: (a) blank; (b) 0.5 wt%NWT; (c) 1 wt%NWT; (d) 3 wt%NWT; (e) 5 wt%NWT; (f) 10 wt%NWT; (g) P25.

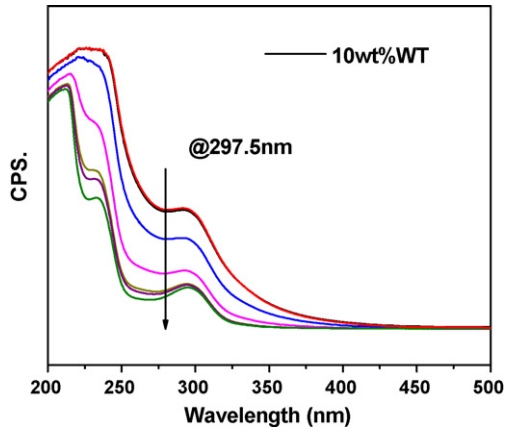

Fig. 12. The adsorption curves of SSA during the photodegradation process using 10 wt%NWT in water at pH value of 5.

Table 4
Initial concentration of SSA solution (C_0), photodegradation rates (($C_0 - C$)/C_0), and the amount of SSA absorbed on the samples (Abs.%)

Samples	C_0	$(C_0 - C)/C_0$ (%)	Abs.%
0.5 wt%NWT	38.3	5.0	4.3
1 wt%NWT	39.02	2.9	2.5
3 wt%NWT	35.43	49.0	11.4
5 wt%NWT	35.08	9.6	12.3
10 wt%NWT	30.47	67.1	23.8
P25	35.64	9.85	10.9
Blank	–	2.1	–

Therefore the nitrogen incorporated process could also occur during MA process.

Urea functioned as a nitrogen source in our experiments. Yin and co-workers [41] suggested that NH_3 could be released from the urea in MA process according to the following reactions:

$$2(NH_2)_2CO \rightarrow NH_3 + NH_2CONHCONH_2\ (\text{biuret}) \quad (1)$$

$$3(NH_2)_2CO \rightarrow 3NH_3 + C_3H_3N_3O_3\ (\text{cyanuric acid}) \quad (2)$$

However, no further explanation on the formation of Ti–N bond by ball-milling was given out. It can be assumed that both NH_3 and the defects, such as oxygen vacancies, formed during ball-milling process should contribute to the nitrogen doping. NH_3 should be absorbed on the surface and interface of TiO_2, and released active [N] and [H] under high pressure. Both the active [N] and [H] can diffuse faster through the defects created by MA, and function quite differently: [H] can react with oxygen in the lattice to produce new oxygen vacancies, and reduce the Ti^{4+} to Ti^{3+} as well, while an active [N] could occupy the position of an oxygen vacancy or served as an interstitial atom. As a result, nitrogen is doped into the lattice of TiO_2, the O–Ti–O bond is changed into O–Ti–N bond, forming oxygen vacancies, F-centers and Ti^{3+} sites as well.

4.2. Mechanism of visible light sensitivity of (W, N) co-doped TiO_2 NPs

As to the origin of visible light photocatalytic activity of the (W, N) co-doped TiO_2 NPs, it can be attributed to the interactions of N-doping, W-doping and the oxygen vacancies formed in the preparing processes. According to the previous reports, doping with W may enlarge the adsorption spectra of TiO_2 because of the formation of a donor state under the conduction band of TiO_2. There were also quite a lot of literatures that focused on the N-doped TiO_2 [42–44]. Based on the first-principle calculation, Asahi et al. [12] concluded that nitrogen was doped into the substitutive sites of TiO_2, and the N 2p accepter states contributed to the band gap narrowing by mixing with O 2p states. Hashimoto and co-workers [42] suggested that oxygen atom in the TiO_2 lattice was substituted by nitrogen atom, and a narrow substitute N 2p band was formed above O 2p valance band. As a result, the binding energy of TiO_2 was lowered by a significant shift. Hashimoto also attributed the lowering of binding energy possibly due to the larger lattice strain after nitrogen doping. Noda et al. [43], who synthesized the N-doped TiO_2, proposed that oxygen vacancies were the cause for the visible light response. Recently, using the spin-polarized plane-wave pseudo-potential method based on the density-function theory, Lin et al. [44] calculated the electron band structure and the optical absorption spectra of N-doped and oxygen-deficient anatase TiO_2. They concluded that the optical absorption of N-doped TiO_2 in the visible light region primarily located between 400 and 500 nm, while that of oxygen-deficient TiO_2 ranged above 500 nm.

The absorption edge of the (W, N) co-doped TiO_2 NPs is above 500 nm in our experiment, as shown in Fig. 6 and Table 2. According to Lin et al. [44], oxygen vacancies should

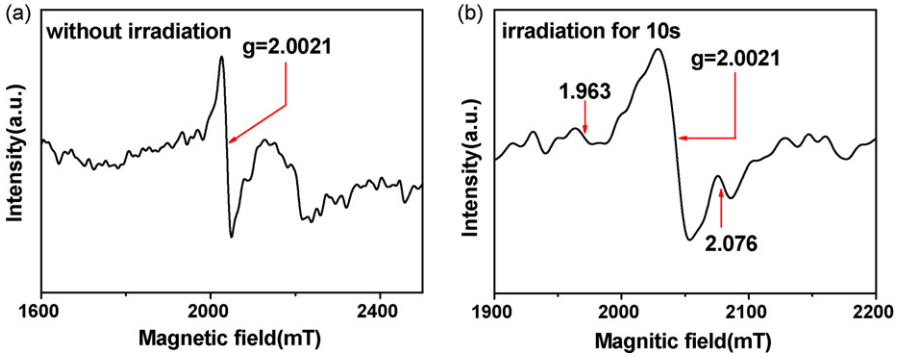

Fig. 13. ESR spectra of 0.5 wt%NWT recorded at 298 K: (a) in dark; (b) irradiation for 10 s with visible light.

contribute mainly for the optical absorption in this region. Therefore ESR spectra were investigated to improve the existence of oxygen vacancies in our samples.

The typical ESR spectra of 0.5 wt%NWT with and without visible light irradiation, registered at 298 K, are shown in Fig. 13. Before the visible light irradiation, there was only one signal with $g = 2.0021$, attributing to the electron trapped on the oxygen vacancy [45]. After the sample was irradiated with visible light for 10 s, three signals appeared in the ESR spectrum. One was the characteristic of Ti^{3+} ions in the TiO_2 matrix with $g = 1.963$, another with $g = 2.0021$ resulted from the electron trapped on the oxygen vacancy (F-centers), and the third with $g = 2.076$ was also due to the O^{2-} radicals [46]. It should be pointed out that the symmetric signal at $g = 2.002$ was noticed by some investigators as F^- or S^- centers [45,47].

5. Conclusions

1. (W, N) co-doped TiO_2 NPs were synthesized by a two-step method, which combined with the sol–gel and the mechanical alloying method.
2. The (W, N) co-doped TiO_2 NPs can induce strong visible light photo-response, and the absorption edge of the co-doped TiO_2 NPs can be red-shifted as far as 650 nm. Besides, the photocatalytic activities of the (W, N) co-doped TiO_2 NPs under visible light irradiation were enhanced greatly compared to those of Degussa P25. In the experiment of photodiscoloration of MB, the color-bleaching rate of the 3 wt%NWT is 2.81 times higher than that of Degussa P25, and the COD_{Cr} removing rate is 1.43 times as high as that of P25. In the experiment of photodegradation of SSA, the photodegradation rate of 10 wt%NWT is about 7 times that of Degussa P25.
3. The donor level formed by W-doping, the acceptor level induced by N-doping and the F-center caused by oxygen vacancies all make contributions to the visible light response of the (W, N) co-doped TiO_2 NPs.

References

[1] V. Palmisano, L. Augugliaro, A. Sclafani, M. Schiavello, J. Phys. Chem. 92 (1988) 6710.
[2] J.C. Yu, J. Yu, W. Ho, Z. Jiang, L. Zhang, Chem. Mater. 14 (2002) 3808.
[3] H. Luo, T. Takata, Y. Lee, J. Zhao, K. Domen, Y. Yan, Chem. Mater. 16 (2004) 846.
[4] Z. Ding, G.Q. Lu, P.F. Greenfield, J. Phys. Chem. B 104 (2000) 4815.
[5] M.R. Hoffmann, S.T. Martin, W. Chio, et al. Chem. Rev. 95 (1995) 69.
[6] N. Serpone, J. Photochem. Photobiol. A 104 (1997) 1.
[7] W. Chio, A. Termin, M.R. Hoffmann, J. Phys. Chem. 98 (1990) 13669.
[8] Y.Q. Wang, H.M. Cheng, L. Zhang, et al. J. Mol. Catal. A 151 (2000) 205.
[9] W. Choi, A. Termin, M.R. Hoffmann, J. Phys. Chem. 98 (1994) 13669.
[10] S. Sakthivel, H. Kisch, Angew. Chem. Int. Ed. 42 (2003) 4908.
[11] T. Tachikawa, S. Tojo, K. Kawai, M. Endo, M. Fujitsuka, et al. J. Phys. Chem. B 108 (2004) 19299.
[12] R. Asahi, T. Morikawa, T. Ohwaki, A. Aoki, Y. Taga, Science 193 (2001) 269.
[13] T. Morikawa, R. Asahi, T. Ohwaki, K. Aoki, Y. Taga, Jpn. J. Appl. Phys. 40 (2001) L561.
[14] S. Sakthivel, H. Kisch, Chem. Phys. Chem. 4 (2003) 487.
[15] T. Ohno, T. Mitsui, M. Matsumura, Chem. Lett. 32 (2003) 364.
[16] Q.W. Zhang, J. Wang, S. Yin, T. Sato, F. Saito, J. Am. Ceram. Soc. 87 (2004) 1161.
[17] T. Yamaki, T. Sumita, S. Yamamoto, J. Mater. Sci. Lett. 21 (2002) 33.
[18] J.C. Yu, L.Z. Zhang, Z. Zheng, J.C. Zhao, Chem. Mater. 15 (2003) 2280.
[19] Y. Sakatani, H. Ando, K. Okusako, H. Koike, J. Nunoshige, T. Takata, J.N. Kondo, M. Hara, K. Domen, J. Mater. Res. 29 (2004) 2100.
[20] J.S. Wang, S. Yin, M. Komatsu, Q.W. Zhang, F. Saito, T. Sato, J. Photochem. Photobiol. A: Chem. 165 (2004) 149.
[21] K. Demeestere, J. Dewulf, H. Van Langenhove, B. Sercu, Chem. Eng. Sci. 58 (2003) 2255.
[22] Chinese National Standard, GB 11914-89, 1989.
[23] J.F. Mammones, S.K. Sharma, M. Nicol, Solid State Commun. 34 (1980) 799.
[24] R.J. Betsch, H.L. Park, W.B. White, Mater. Res. Bull. 26 (1991) 613.
[25] Y.H. Zhang, C.K. Chan, J. Porter, W.J. Guo, J. Mater. Res. 13 (1998) 2602.
[26] U. Balachandran, N.G. Eror, J. Solid State Chem. 42 (1982) 276.
[27] M.F. Daniel, B. Desbat, J. Lassegues, B. Gerand, M. Figlarz, J. Solid State Chem. 67 (1987) 235.
[28] K. Chhor, J.F. Bocquent, C. Pommier, Mater. Chem. Phys. 32 (1992) 249.
[29] R. Urlaub, U. Posset, R.F.T. Thull, J. Non-Cryst. Solids 265 (2000) 276.
[30] T. Bezrodna, G. Puchkovska, V. Shimanovaska, I. Chashecnnikva, T. Khalyavaka, J. Baran, Appl. Surf. Sci. 214 (2003) 222.
[31] R.M. Silverstein, G.C. Bassler, T.C. Morrill, Spectrometric Identification of Organic Compounds, 4th ed., John Wiley and Sons, Inc., New York, 1981.
[32] K.S.W. Sing, D.H. Everett, R.A.W. Haul, L. Moscou, R.A. Pierotti, J. Rouquerol, T. Siemieniewska, Pure Appl. Chem. 57 (1985) 603.
[33] H.M. Luo, C. Wang, Y.S. Yan, Chem. Mater. 15 (2003) 3814.
[34] X.B. Chen, C. Burda, J. Phys. Chem. B 108 (2004) 15446.
[35] T. Sano, N. Negishi, K. Koike, K. Takeuchi, S. Matsuzawa, Mater. Chem. 14 (2004) 380.
[36] O. Diwald, T.L. Thompson, E.G. Goralski, S.D. Walck, J.T. Yates, J. Phys. Chem. B 14 (2004) 380.
[37] Y. Aita, M. Komatsu, S. Yin, T. Sato, J. Solid State Chem. 177 (2004) 3235.
[38] S. Sakthivel, M. Jamczarek, H. Kisch, J. Phys. Chem. B 108 (2004) 19384.
[39] J.L. Gole, J.D. Stout, C. Burda, Y.B. Lou, X.B. Chen, J. Phys. Chem. B 108 (2004) 1230.
[40] C. Suryanarayana, Prog. Mater. Sci. 46 (2001) 1.
[41] J.S. Wang, S. Yin, M. Komastsu, Q.W. Zhang, F. Saito, T. Sati, Appl. Catal. B: Environ. 52 (2004) 11.
[42] H. Irie, Y. Watanabe, K. Hashimoto, J. Phys. Chem. B 107 (2003) 5483.
[43] H. Noda, K. Oikawa, T. Ogata, K. Matsuki, H. Kamata, Chem. Soc. Jpn. 8 (1986) 1084.
[44] Z.S. Lin, A. Orlov, R.M. Lambert, M.C. Payne, J. Phys. Chem. B 109 (2005) 20948.
[45] A.M. Volodin, A.E. Cherkashin, V.S. Zakharenko, React. Kinet. Catal. Lett. 11 (1979) 107.
[46] E. Serwicka, Colloids Surf. 13 (1985) 287.
[47] P.F. Cornaz, J.H.C. Van Hooff, F.J. Pluijm, G.C.A. Schuit, Disc. Faraday Soc. 41 (1966) 290.